Quantum signatures of non-Newtonian orbits in the asymmetric infinite square well

Todd K. Timberlake* and Molly M. Nelson
Department of Physics, Astronomy, and Geology, Berry College, Mount Berry, Georgia 30149-5004, USA
(Received 2 January 2009; published 31 March 2009)

An infinite square well with a rectangular step is one of the simplest systems to exhibit non-Newtonian ray-splitting periodic orbits in the classical limit. We examine eigenvalue spacings in the quantum version of this system. The sequence of spacings shows deviations from uniformity at energies just above the step height and distinct resonance features are visible at certain energies. Semiclassical analysis shows that these features are directly related to the presence of non-Newtonian orbits in the classical system. In addition, the resonance features are shown to produce revivals in suitably constructed wave packets peaked at the resonance energy.

DOI: 10.1103/PhysRevE.79.036213 PACS number(s): 05.45.Mt, 03.65.Sq, 42.50.Md

I. INTRODUCTION

During the last 30 years important links have been found between the properties of quantum eigenvalues and the dynamics of the corresponding classical system. In 1977 Berry and Tabor [1] proposed that energy eigenvalues in generic quantum systems with integrable classical counterparts follow Poisson statistics after unfolding. In 1984 Bohigas *et al.* [2] proposed that the unfolded energy eigenvalues of a quantum system with chaotic classical counterpart will follow random matrix statistics. Further studies have, for the most part, confirmed these hypotheses. One exception is that unfolded eigenvalues of quantum systems with a single degree of freedom typically display uniform spacing [3]. For chaotic systems an important link between quantum eigenvalues and classical dynamics was forged with the development of periodic-orbit theory [4]. The centerpiece of periodic-orbit theory is the Gutzwiller trace formula which relates the quantum density of states to the periodic orbits of the classical system. In general the trace formula gives only approximate results, becoming exact in the limit $\hbar \to 0$. However, for some systems the periodic-orbit theory is exact even for finite $\hbar$ [5]. These results and others from the field of quantum chaos are surveyed in several recent monographs [3,4,6,7].

Recently the study of the connections between quantum eigenvalues and classical dynamics has been extended to the case of ray-splitting systems. In the semiclassical limit ($\hbar \to 0$) the wavelength of the quantum particle is usually taken to be small compared to all relevant length scales in the classical system, so the quantum wave equations reduce to ray equations (i.e., Hamilton's equations of motion for conservative systems). Ray-splitting systems are systems in which the potential changes significantly on length scales that are small compared to the wavelength of the quantum particle even in the semiclassical limit $\hbar \to 0$, as when there is a discontinuous change in the potential within the region accessible to the particle. In the semiclassical limit, a particle in a ray-splitting system will exhibit raylike (Newtonian) behavior everywhere except at the discontinuous boundary. At the boundary the ray may split, with one part of the ray transmitted across the boundary and the other part reflected from the boundary. This ray-splitting results in non-Newtonian periodic orbits that can influence the quantum dynamics. Gutzwiller's trace formula has been extended to ray-splitting systems [8]. Recent numerical and experimental studies of two-dimensional ray-splitting billiards have revealed signatures of non-Newtonian periodic orbits in the Fourier transform of the quantum density of states [9–14], the distribution of level spacings [10,15], and the scarring of energy eigenstates [9,10,12,14].

The purpose of the current study is to examine quantum signatures of non-Newtonian orbits in the simplest possible system: the asymmetric infinite square well (AISW). The AISW consists of an infinite square well with a rectangular step at the center of the well. The potential energy function is

$$V(x) = \begin{cases} \infty, & |x| \geq a \\ 0, & -a < x \leq 0 \\ V_0, & 0 < x < a. \end{cases} \tag{1}$$

From elementary quantum mechanics we know that a plane wave with energy $E > V_0$ incident on the boundary at $x=0$ may be reflected with probability r^2 or transmitted with probability $1-r^2$, where

$$r = \frac{1 - \sqrt{1 - V_0/E}}{1 + \sqrt{1 - V_0/E}}. \tag{2}$$

Since r does not depend on $\hbar$ this ray-splitting phenomenon persists in the semiclassical limit $\hbar \to 0$. As a result, the classical dynamics contains non-Newtonian periodic orbits such as those shown in Fig. 1. The orbit p_1 is the usual Newtonian orbit that moves back and forth between the infinite walls at $x = \pm a$. The orbit p_2 is a non-Newtonian orbit that is confined to the left side of the well, reflecting each time it reaches the boundary at $x=0$ from the left. Similarly the orbit p_3 is confined to the right side of the well and reflects each time it reaches the boundary at $x=0$. An infinite variety of other non-Newtonian orbits, corresponding to combinations of the three basic orbits described above, are also possible. Non-Newtonian orbits are also possible for $E < V_0$. In this case the non-Newtonian orbits explore the classically-forbidden right side of the well. Our analysis will focus on $E > V_0$, so we will not explore these so-called "ghost orbits" in any detail.

*ttimberlake@berry.edu

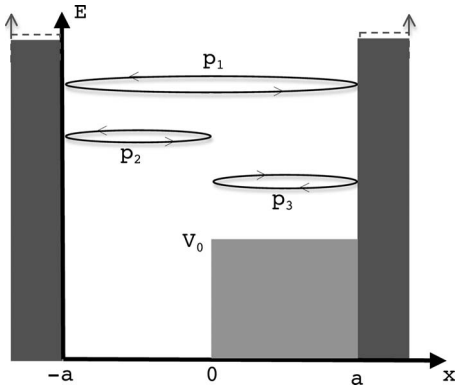

FIG. 1. Periodic orbits in the asymmetric infinite square well. The Newtonian orbit p_1 bounces back and forth between the hard walls at $x=\pm a$. The non-Newtonian orbits p_2 and p_3 are confined to the left and right sides of the well, respectively. These orbits reflect each time they reach the discontinuity in the potential at $x=0$.

The energy eigenfunctions for the AISW have been investigated in Refs. [16,17]. Here we will examine the sequence of energy eigenvalues in order to illustrate properties of the eigenvalue sequence that are related to non-Newtonian orbits in the classical system. In Sec. II we present a method for finding energy eigenvalues of the AISW, discuss the procedure for unfolding these eigenvalues, and examine the spacings between consecutive eigenvalues in the sequence. The level spacing sequence shows nonuniformity in a range of energies just above V_0 and striking resonance features at specific energies in this range. These properties of the level spacing sequence are shown to be related to classical non-Newtonian periodic orbits in Sec. III. In Sec. IV we show that the resonance features in the level spacing sequence give rise to partial revivals for specially constructed wave packets peaked at the resonance energy. Section V provides a summary and discussion of our results.

II. PROPERTIES OF THE EIGENVALUE SEQUENCE

For $E>V_0$ the energy eigenstates for the AISW are of the form

$$\psi(x)=\begin{cases} A\sin[Q(x+a)] & \text{for } -a<x\le 0 \\ B\sin[q(x-a)] & \text{for } 0<x<a, \end{cases} \tag{3}$$

where $Q\equiv\sqrt{2mE}/\hbar$ and $q\equiv\sqrt{2m(E-V_0)}/\hbar$. Requiring ψ and $d\psi/dx$ to be continuous at $x=0$ leads to the energy eigenvalue equation:

$$Q\cos(Qa)\sin(qa)+q\cos(qa)\sin(Qa)=0. \tag{4}$$

To find the energy eigenvalues for a given value of V_0 we make use of a procedure introduced in Ref. [18]. First we define the classical action length, $S(E)$, for a particle with energy $E>V_0$ moving across the well:

$$S(E)=a\sqrt{2mE}+a\sqrt{2m(E-V_0)}. \tag{5}$$

Inverting this equation we obtain

$$E(S)=(S^2+2ma^2V_0)^2/(8S^2a^2m). \tag{6}$$

As shown in Ref. [18], each energy eigenvalue of the AISW falls between a pair of *energy separators*

$$\hat{E}_n=E(\pi\hbar(n-1/2)). \tag{7}$$

Since the nth energy eigenvalue E_n will always be bracketed in the interval $(\hat{E}_n,\hat{E}_{n+1})$ we can use a simple bisection method to solve Eq. (4) and rapidly converge to the value for E_n [19].

Once we have obtained the sequence of energy eigenvalues we can examine the spacings between adjacent energies. Before we can examine the spacings, though, we must account for any systematic variation in the mean spacing throughout the sequence. We wish to examine how the spacings vary about the mean, not how the mean spacing itself varies. In general the mean spacing between adjacent energy eigenvalues will depend on the energy. For example, in the infinite square well the level spacing increases linearly with energy. To account for the energy dependence of the mean spacing we must *unfold* the eigenvalues. The unfolding procedure rescales the eigenvalues so that their mean spacing is one throughout the entire sequence. To unfold the eigenvalues we use the average level staircase function, $\bar{N}(E)$, which gives the average number of energy eigenvalues less than E. For the AISW we have [18]

$$\bar{N}(E)=S(E)/(\pi\hbar)-\gamma_0, \tag{8}$$

where $S(E)$ is given in Eq. (5) and γ_0 is a small correction term (which we will ignore since it has no impact on the level spacings). The unfolded eigenvalues are then $\epsilon_n=\bar{N}(E_n)\approx n$.

To investigate a sequence of eigenvalues numerically we must first choose values for our parameters. We define a set of length, mass, and time units such that $\hbar=1$, $m=1/2$, and $a=3$. We set $V_0=100\,000$ in the corresponding units of energy. We choose this large value for V_0 in order to have many energy eigenvalues with $E>V_0$ but also $E/V_0\approx 1$. It is for this range of energies that the reflection coefficient r [Eq. (2)] is both real and of order 1, and therefore non-Newtonian ray-splitting orbits can be expected to play a significant role. We computed the first 1500 energy eigenvalues above the step $(E_n>V_0)$ for this set of parameter values using the procedure described above. To check our unfolding procedure we inverted the sequence to find $N(E)$ and compared the numerical results with the average staircase function $\bar{N}(E)$ given in Eq. (8). The results are shown in Fig. 2. The average level staircase function $\bar{N}(E)$ is indistinguishable from the numerically computed $N(E)$, so we can be confident in our use of $\bar{N}(E)$ in the unfolding procedure. Note that the curves begin at $N(V_0)=302$, indicating that there are 302 energy eigenvalues below the step for this set of parameters.

Once the sequence of eigenvalues has been unfolded we can examine the spacings, $\epsilon_{n+1}-\epsilon_n$. Figure 3 shows the sequence of spacings for the first 1500 eigenvalues above the step. The sequence of level spacings exhibits several notable features. It is clear that the spacings are nonuniform for en-

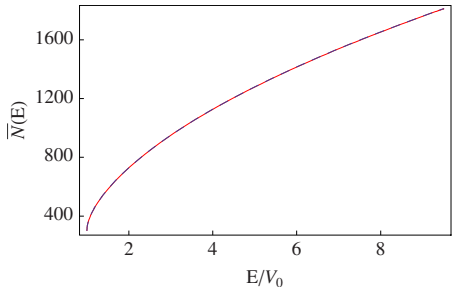

FIG. 2. (Color online) Comparison of the numerically computed staircase function $N(E)$ (solid curve) and the average level staircase function $\bar{N}(E)$ from Eq. (8) (dashed curve). The two curves are indistinguishable on the scale of this plot.

ergies just above the step. The unfolded eigenvalues of simple one-dimensional quantum wells are expected to exhibit uniform spacing (with all spacings equal to one). The spacings for the AISW do appear to converge toward one at high energies, but for energies just above the step there is a significant amount of scatter. However, there is some structure in the sequence of level spacings even at energies just above the step. All of the spacings are contained between two well-defined curves, both of which approach one (from opposite directions) at high energies. At certain energies the scatter of points seems to coalesce into a small number of distinct subsequences. For example, near $i=523$ (corresponding to an energy $E\approx 4V_0/3$) the sequence of spacings consists of three well-defined subsequences.

In the following section we will use semiclassical analysis to relate these properties of the sequence of spacings to non-Newtonian periodic orbits. But before turning to that analysis we would like to briefly mention the presence of avoided crossings in the eigenvalue spectrum for the AISW. Figure 4 shows the sequence of energy eigenvalues E as a function of the step height V_0. The step height ranges from an initial value of $V_0^i=100\,000$ (in the energy units we have chosen) up to $1.02V_0^i$. The horizontal dashed lines in Fig. 4 show the energy eigenvalues for a particle confined to the left side of the well (i.e., a particle in an infinite square well with hard walls at $x=-a$ and $x=0$). Eigenvalues above the step generally increase with V_0. A clear transition is visible whenever an eigenvalue falls below V_0, which occurs when V_0 is approximately halfway between eigenvalues for the left-side well. Once an eigenvalue has fallen below V_0 it increases

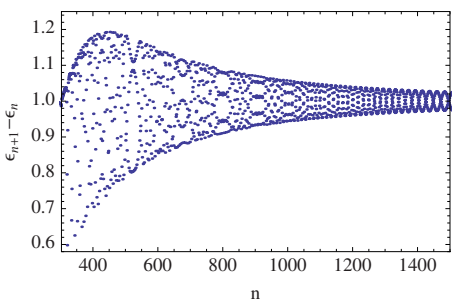

FIG. 3. (Color online) Spacings between consecutive unfolded eigenvalues for the AISW with $a=3$ and $V_0=100\,000$. The plot shows the spacings for the first 1500 levels above the step.

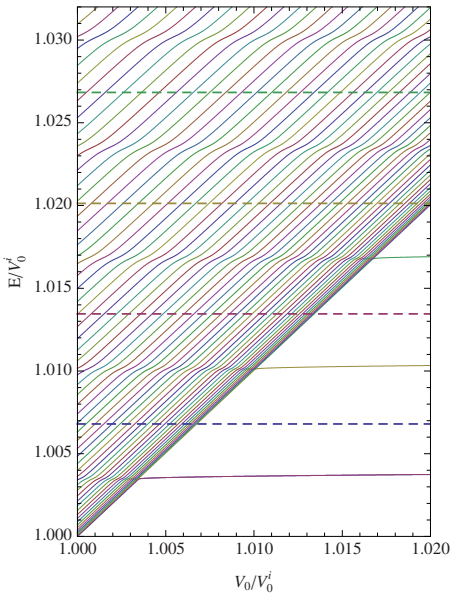

FIG. 4. (Color online) Eigenvalue curves for the AISW as a function of V_0. The initial value of V_0 is $V_0^i=100\,000$ in the energy units we have chosen. The solid curves show the energy eigenvalues of the AISW as a function of V_0. The horizontal dashed lines show the energy eigenvalues of a particle confined to the left side of the well. Note the series of avoided crossing at the energies for which an eigenvalue falls below V_0 (which occurs about halfway between the eigenvalues of the left-side well).

only gradually, asymptotically approaching an eigenvalue of the left-side well as $V_0\to\infty$. Each eigenvalue curve above the step goes through an avoided crossing when it passes through one of the transition energies at which one of the eigenvalues falls below V_0. The appearance of avoided crossings is associated with changes in level spacing statistics and other aspects of quantum chaos [20]. However, it should be noted that the avoided crossings in this system are of a very peculiar sort, occurring only at specific energies. A more detailed investigation of avoided crossings in the AISW lies outside of the scope of this paper.

III. SEMICLASSICAL ANALYSIS

In this section we use semiclassical analysis to connect the features of the level spacing sequence observed in Sec. II to non-Newtonian periodic orbits in the classical system. A semiclassical analysis of the AISW was carried out by Dabaghian and Jensen [18]. They showed that exact energy eigenvalues for the AISW can be calculated using an infinite sum over the (Newtonian and non-Newtonian) periodic orbits of the classical system. The procedure they used is not convergent for $E<V_0$ [21]. An exact, convergent semiclassical formula for $E<V_0$ can be obtained by accounting for ghost orbits (orbits that exist in the right side of the well, which is forbidden in Newtonian mechanics) [5,21]. Here we will avoid using ghost orbits by confining our attention to $E>V_0$.

The semiclassical formula for the unfolded energy eigenvalues of the AISW (with $\hbar=1$) is [18]

$$\epsilon_n = n - \frac{1}{2} - \omega_n, \tag{9}$$

where

$$\omega_n \equiv \frac{1}{\pi^2}\mathrm{Im}\sum_{p,\nu}\int_{\pi(n-1/2)}^{\pi(n+1/2)} \frac{A_p^\nu}{\nu} e^{i\nu S_p} dS. \tag{10}$$

The variable S is the classical action length given in Eq. (5). The index p labels all of the (Newtonian or non-Newtonian) periodic orbits and S_p is the classical action of the orbit p. Since any periodic orbit p consists of n_1 left-side orbits (such as p_2 in Fig. 1) and n_2 right side orbits (such as p_3 in Fig. 1), we have $S_p = 2n_1S_1 + 2n_2S_2$, where

$$S_1 = a\sqrt{2mE} \text{ and } S_2 = a\sqrt{2m(E - V_0)}. \tag{11}$$

The index ν accounts for repetitions of a given orbit p. The factor A_p is a weighting factor given by

$$A_p = (-1)^{\chi(p)} r^{\sigma(p)} t^{\tau(p)}, \tag{12}$$

where $t^2 = 1 - r^2$, $\sigma(p)$ counts the number of times the orbit p reflects from the barrier at $x=0$, $\tau(p)$ counts the number of times the orbit transmits through the barrier, and $\chi(p)$ counts the combined number of reflections from the hard walls and right reflections from the boundary (each of which results in a sign change in the particle's wave function). A more detailed discussion of this formula can be found in Ref. [18].

The spacings between consecutive unfolded eigenvalues are

$$\epsilon_{n+1} - \epsilon_n = 1 - (\omega_{n+1} - \omega_n). \tag{13}$$

It is clear that any nonuniformities in the level spacing must be due to the oscillatory terms ω_n. These oscillatory terms involve a sum over all periodic orbits, both Newtonian and non-Newtonian. To separate out the contributions of these two types of orbits we begin by examining the contribution to ω_n from the Newtonian orbit. In this case $S_p = 2S$ (since the Newtonian orbit crosses the entire well in *both* directions) and $A_p = t^2$ [because for the Newtonian orbit $\sigma(p)=0$, $\tau(p)=2$, and $\chi(p)=2$], so the contribution of this orbit to ω_n is

$$\frac{1}{\pi^2}\mathrm{Im}\sum_{\nu}\int_{\pi(n-1/2)}^{\pi(n+1/2)} \frac{t^{2\nu}}{\nu} e^{i2\nu S} dS. \tag{14}$$

If we approximate t as a constant in the interval $\pi(n-1/2) < S < \pi(n+1/2)$ we find that

$$\frac{1}{\pi^2}\mathrm{Im}\sum_{p,\nu}\frac{t^{2\nu}}{\nu}\int_{\pi(n-1/2)}^{\pi(n+1/2)} e^{i2\nu S} dS = 0. \tag{15}$$

For larger values of E, t will be approximately constant over the interval of integration and thus the Newtonian orbit will not contribute to the sum in ω_n. At energies just above V_0, t cannot be treated as a constant over the integration interval, but even in this case numerical evaluation of the Newtonian orbit's contribution to ω_n shows that it does not account for the nonuniformity seen in the level spacings. In particular, using the parameter values given in Sec. II we find that the maximum value of

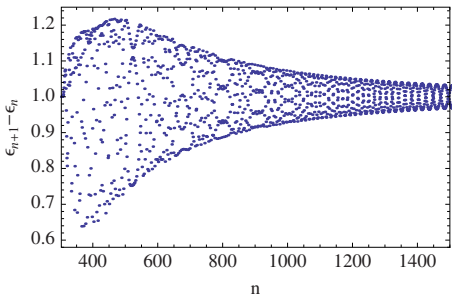

FIG. 5. (Color online) Level spacings computed using the semiclassical formula in Eq. (13). Only contributions from short non-Newtonian orbits were included. The results show good agreement with the numerically computed spacings in Fig. 3.

$$\frac{1}{\pi^2}\mathrm{Im}\int_{\pi(n-1/2)}^{\pi(n+1/2)} t^2 e^{i2S} dS \tag{16}$$

for any n is less than 7×10^{-4}. The contribution for higher values of ν are even smaller. Thus it appears that the Newtonian orbit (and its repetitions) do not account for the nonuniformity of the spacings seen in Fig. 3. We therefore conclude that the nonuniformity in the spacings is due to the presence of non-Newtonian orbits.

To confirm this conclusion we have computed the semiclassical level spacings using Eq. (13). We included in our computations only the contributions from the shortest non-Newtonian orbits. We included the orbit that is confined to the left side of the well (shown as p_2 in Fig. 1) and its $\nu=2$ repetition as well as the orbit that is confined to the right side of the well (p_3 in Fig. 1) and its $\nu=2$ repetition. No other contributions were included in the computation. The results are shown in Fig. 5. Comparison of these results with the numerically computed spacings shown in Fig. 3 makes it clear that the nonuniformity in the level spacings is due primarily to these short non-Newtonian orbits. The semiclassical spacings are very similar to the numerically computed spacings with the difference being greatest for energies just above the step. In particular, the semiclassical spacings show all of the principal features of Fig. 3, including the convergence to uniform spacing at high energies and the appearance of structure in the spacings sequence at certain energies.

The convergence to uniform spacing at high energy can be easily understood by reference to Eq. (10). We have already established that the Newtonian orbit makes a negligible contribution to ω_n, especially at high energies. However, the contribution from the non-Newtonian orbits is also suppressed at high energy. This is because each non-Newtonian orbit involves at least one reflection, and therefore a factor of r will appear within the factor A_p for each non-Newtonian orbit p. As $E\to\infty$, $r\to0$, so at high energies the non-Newtonian orbits will not contribute to ω_n. So as $E\to\infty$ we expect $\omega_n\to0$ and therefore $(\epsilon_{n+1}-\epsilon_n)\to1$. This fits with the expectation that at very high energies the effect of the step will not be noticeable and the system will behave like the usual infinite square well.

The semiclassical analysis can also be used to explain the structure in the spacings sequence that appears at specific

energies if we make use of a few approximations. We begin by approximating the classical action S_p of the periodic orbit p with a first-order Taylor series in the variable S about $S=S_n$ [where $\pi(n-1/2)<S_n<\pi(n+1/2)$]:

$$S_p(S) \approx S_p(S_n) + \left(\frac{dS_p}{dS}\right)_{S=S_n}(S-S_n) = \alpha_{p,n}S + \beta_{p,n}, \quad (17)$$

where

$$\alpha_{p,n} \equiv \left(\frac{dS_p}{dS}\right)_{S=S_n} \text{ and } \beta_{p,n} \equiv S_p(S_n) - \alpha_{p,n}S_n. \quad (18)$$

We then approximate A_p as a constant on the interval $\pi(n-1/2)<S<\pi(n+1/2)$ so that $A_p(S)\approx A_p(S_n)=A_{p,n}$ and

$$\int_{\pi(n-1/2)}^{\pi(n+1/2)} \frac{A_{p,n}^{\nu}}{\nu} e^{i\nu S_p} dS \approx \frac{A_{p,n}^{\nu}}{\nu} e^{i\nu\beta_{p,n}} \int_{\pi(n-1/2)}^{\pi(n+1/2)} e^{i\nu\alpha_{p,n}S} dS. \quad (19)$$

Evaluating this integral, taking the imaginary part, and substituting into Eq. (10) we find

$$\omega_n \approx \frac{1}{\pi^2}\sum_{p,\nu} \frac{(A_{p,n})^{\nu}}{\nu} \sin(\nu\alpha_{p,n}\pi/2)\sin[\nu(n\pi\alpha_{p,n}+\beta_{p,n})]. \quad (20)$$

Examination of Eq. (20) shows that the energy eigenvalues will break up into a small number of distinct subsequences whenever $\nu\pi\alpha_{p,n}$ is equal to 2π times a rational number with a small denominator. In other words, we need $\alpha_{p,n}/2$ to be a rational number with a small denominator, and the denominator will determine the number of distinct subsequences.

The physical significance of this condition on $\alpha_{p,n}$ becomes clear if we recall the theory of classical action-angle variables, which shows us that

$$\frac{dE}{ds} = \frac{2\pi}{T}, \quad (21)$$

where E is the energy of a classical particle, s is the action of the particle along a closed orbit, and T is the period of that closed orbit. Note that the action length S given in Eq. (5) is actually *half* of the action for a classical particle following the Newtonian periodic orbit (p_1 in Fig. 1). So $s=2S$ and

$$\frac{dE}{dS} = \frac{4\pi}{T}, \quad (22)$$

where here T is the period of the classical Newtonian orbit p_1. Similarly,

$$\frac{dE}{dS_p} = \frac{2\pi}{T_p}, \quad (23)$$

where S_p is the action of the periodic orbit p and T_p is the period of that orbit. We can now use these results to rewrite $\alpha_{p,n}$:

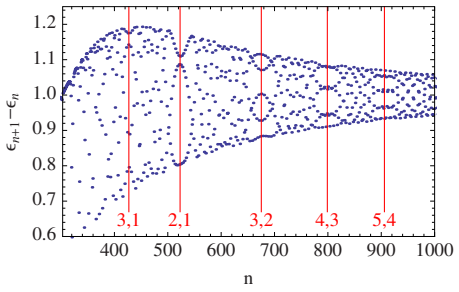

FIG. 6. (Color online) Comparison of the predicted resonance locations with the numerically computed sequence of spacings from Fig. 3. The vertical lines show the predictions of Eq. (30) for various values of (j,k). At each predicted resonance location the sequence of spacing breaks up into $j+k$ distinct subsequences.

$$\alpha_{p,n} = \left(\frac{dS_p}{dS}\right)_{S=S_n} = \left(\frac{dS_p}{dE}\frac{dE}{dS}\right)_{S=S_n} = \left(\frac{dE/dS}{dE/dS_p}\right)_{S=S_n} = \frac{2T_p(S_n)}{T(S_n)}. \quad (24)$$

So $\alpha_{p,n}/2=T_p/T$. But $T_p=n_1T_1+n_2T_2$ and $T=T_1+T_2$, where

$$T_1 = a\sqrt{\frac{2m}{E}} \text{ and } T_2 = a\sqrt{\frac{2m}{E-V_0}}. \quad (25)$$

For T_p/T to be rational for all orbits p it must be that

$$\frac{T_2}{T_1} = \frac{j}{k}, \quad (26)$$

where j and k are integers and $j>k$ (since $T_2>T_1$). It is now clear that the structures seen in the sequence of spacings are resonance phenomena that occur when the periods of the orbits on the left and right sides of the well are rationally related. Specifically, we find that when the condition in Eq. (26) is satisfied we have

$$\frac{\alpha_p}{2} = \frac{T_p}{T} = \frac{n_1k+n_2j}{j+k}, \quad (27)$$

and the sequence of eigenvalues will break up into $j+k$ distinct subsequences.

Using Eq. (25) we can rewrite the resonance condition [Eq. (26)] in terms of the energy E:

$$\sqrt{\frac{E}{E-V_0}} = \frac{j}{k}. \quad (28)$$

Solving this equation for E we find the resonance energies

$$E_{j,k} = \frac{j^2V_0}{j^2-k^2}. \quad (29)$$

We can determine the value of n for which the unfolded spacing $\epsilon_{n+1}-\epsilon_n$ will be near a resonance by applying the unfolding procedure to $E_{j,k}$:

$$n_{j,k} \approx \bar{N}(E_{j,k}). \quad (30)$$

Figure 6 shows a comparison of the predicted resonance locations from Eq. (30) for various (j,k) with the numerically computed sequence of spacings. For the (2, 1) and (3, 2)

cases it is clear that the sequence of spacings breaks up into $j+k$ distinct subsequences at the predicted resonance location. For the other cases there are clearly visible resonances at the predicted locations, but the number of distinct subsequences is hard to see. However, by zooming in on the appropriate regions of the plot we have been able to confirm that all resonances appear at the predicted locations and consist of $j+k$ distinct subsequences. Therefore it appears that the structures seen in the sequence of level spacings can be understood as arising from a resonance between the various non-Newtonian classical periodic orbits.

IV. WAVE-PACKET REVIVALS

In this section we will examine the connection between the resonance phenomena discussed above and wave-packet revivals. A wave-packet revival occurs when a wave packet returns to its original state after initially dispersing. This phenomenon is common in one-dimensional quantum wells. For a quantum harmonic oscillator a wave packet peaked at energy E will return to its initial state at $t=iT_{\mathrm{cl}}$, where i is any integer and T_{cl} is the period of a classical particle with energy E. In an infinite square well of length $2a$ any wave packet peaked at energy E will oscillate with period T_{cl} but will disperse and lose its shape over time. However, the wave packet will return *exactly* to its initial state at $t=iT_{\mathrm{rev}}$, where i is any integer and $T_{\mathrm{rev}}=16ma^2/(\pi\hbar)$ [22]. Other one-dimensional wells give rise to partial revivals in which the wave packet returns close, but not exactly, to its initial shape at regular intervals.

Wave-packet revivals depend sensitively on properties of the energy eigenvalue sequence. The uniform spacing of harmonic oscillator eigenvalues prevents wave packets from dispersing in that system. The linearly increasing spacing between eigenvalues in the infinite square well leads to periodic exact revivals in that system. Other systems can produce partial revivals for wave packets that are well localized in energy because the energy eigenvalue function $E_n=f(n)$ can be locally approximated with a first-order Taylor series and thus the system behaves approximately like an infinite square well over a short range of energies. The scatter of (unfolded) level spacings shown in Fig. 3 would seem to leave little hope that wave-packet revivals would be possible in the AISW at energies just above V_0. However, at a resonance energy the spacings alternate between a small number of distinct subsequences. If we construct a wave packet using only states from one of these sequences, all with energies very close to the resonance energy, then the spacings between the unfolded eigenvalues will be roughly uniform. Such a wave packet might be expected to exhibit partial revivals. Note that even if the spacings within a single subsequence were exactly uniform we would not get harmonic oscillator-type behavior. This is because the spacings in Fig. 3 are between unfolded eigenvalues. The spacings between the actual eigenvalues (before unfolding) will not be uniform, but they will be approximately linear in n near the resonance energy.

To test this hypothesis we examine the behavior of specially constructed wave packets in the AISW with the parameter values given in Sec. II. We begin by constructing a Gaussian wave packet centered at the resonance energy $E_{2,1}=4V_0/3$:

$$\Psi(x,0)=\left(\frac{1}{\rho^2\hbar^2\pi}\right)^{1/4}\exp\left[-\frac{ip_0(x-x_0)}{\hbar}-\frac{(x-x_0)^2}{2\rho^2\hbar^2}\right]. \tag{31}$$

To ensure that the wave packet is peaked at energy $E_{2,1}$ we choose $p_0=\sqrt{2mE_{2,1}}$. We also choose $x_0=-a/2$ and $\rho=1/4$ in units of reciprocal momentum. We expand this wave function in terms of the energy eigenstates $\psi_n(x)$ [given by Eq. (3) with Q and q evaluated at $E=E_n$] to get

$$\Psi(x,0)=\sum_n c_n\psi_n(x), \tag{32}$$

where

$$c_n=\int_{-a}^{a}\Psi(x,0)\psi_n^*(x)dx. \tag{33}$$

In general $\Psi(x,0)$ will have support on all of the eigenstates with energies close to the resonance energy. To project onto a single resonance subsequence we simply retain the terms from Eq. (32) with

$$\mathrm{mod}(n,3)=k,\quad k=0,1,2, \tag{34}$$

set all other c_n's to zero and renormalize the resulting wave function. In this way we get three different wave packets corresponding to the three values of k in Eq. (34), each of which has support on only one of the resonance subsequences.

To study the revival behavior of a wave packet we examine the autocorrelation function

$$A(t)=\int_{-a}^{a}\Psi^*(x,t)\Psi(x,0)dx. \tag{35}$$

This quantity measures the overlap of the initial wave packet with the wave packet at time t. A perfect revival would result in $|A(t)|^2=1$. A plot of $|A(t)|^2$ will show sharp peaks at any time during which a revival occurs. Figure 7 shows $|A(t)|^2$ for our three specially constructed wave packets as well as for the full Gaussian wave packet. Note that the time is given in multiples of the classical period

$$T_{\mathrm{cl}}=a\sqrt{\frac{2m}{E}}+a\sqrt{\frac{2m}{E-V_0}}, \tag{36}$$

where in this case $E=E_{2,1}=4V_0/3$. Figures 7(a)–7(c) show evidence of partial revivals equally spaced in time although there is a decay in the quality of each subsequent revival. Note that the revival times for these three wave packets are all different. This difference explains why the full Gaussian wave packet [shown in Fig. 7(d)] does not show any revival behavior. Because the three wave packets with support on a single subsequence have revivals at slightly different times it is impossible for the full Gaussian wave packet, which is a combination of the other three, to experience a revival at any time.

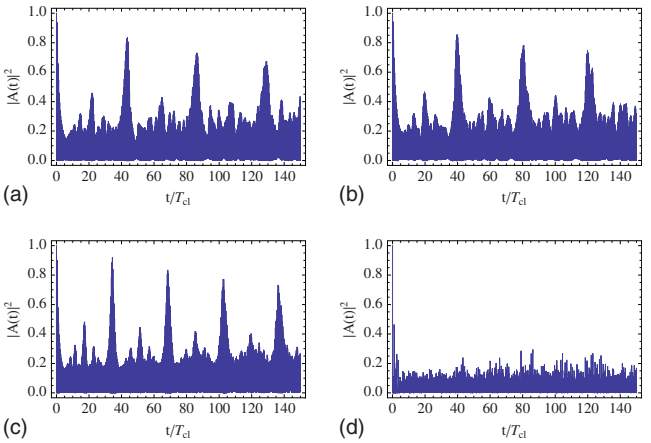

FIG. 7. (Color online) Autocorrelation function $A(t)$ for wave packets centered at the resonance energy $E_{2,1}=4V_0/3$. The plots show $|A(t)|^2$ for (a)–(c) a Gaussian wave packet projected onto every third eigenstate and (d) the full Gaussian wave packet. Partial revivals are clearly visible for the wave packets constructed using every third state.

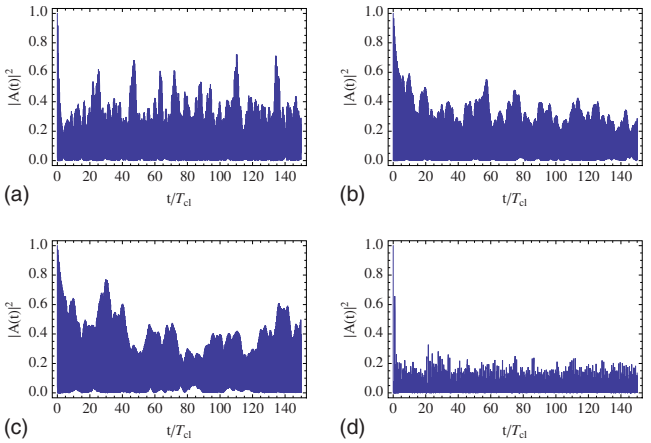

FIG. 8. (Color online) Autocorrelation function $A(t)$ for wave packets centered at the off-resonance energy $E=1.47V_0$. The plots show $|A(t)|^2$ for (a)–(c) a Gaussian wave packet projected onto every third eigenstate and (d) the full Gaussian wave packet. There is no visible pattern of revival peaks in any of the plots.

To show that this revival behavior is really a product of the resonances in the level spacing we have also computed $|A(t)|^2$ for wave packets constructed as described above but centered on an energy ($E=1.47V_0$) that is outside any of the resonance regions. The results are shown in Fig. 8. It is clear that none of these wave packets exhibits periodic revivals.

V. SUMMARY AND CONCLUSIONS

We have examined the spacings between unfolded energy eigenvalues in the asymmetric infinite square-well system. The spacings are nonuniform for a range of energies above the step, converging to the uniformity expected of one-dimensional quantum wells as $E\to\infty$. Within the nonuniform spacings there are regions of structure at certain energies where the scattered spacings coalesce into a small number of distinct subsequences. Using semiclassical analysis we have shown that the nonuniformity in the level spacings is due the influence of short non-Newtonian periodic orbits in the classical system. We have also shown that the structures seen in the spacing sequence are due to resonances between non-Newtonian periodic orbits confined to the left and right sides of the well. Finally, we have shown that these resonance features lead to partial revivals in specially constructed wave packets peaked near the resonance energy.

All of the numerical results presented in this paper are for a single set of parameters (given in Sec. II). We have also investigated the AISW for other parameter sets, including other values of V_0 and for

$$V(x)=\begin{cases}\infty, & x\le -a\\ 0, & -a<x\le 0\\ V_0, & 0<x<b\\ \infty, & x\ge b,\end{cases} \tag{37}$$

where $b\neq a$. In all cases we found behavior qualitatively similar to that presented in this paper.

Although the spacings in the AISW for energies just above the step appear somewhat random, it is not possible to compare the statistical properties of the spacings to those of standard distributions such as the Poisson or Gaussian orthogonal ensemble distributions. This is because the behavior of the spacings is highly energy dependent, changing from nonuniform just above the step to uniform at higher energies. To get around this problem we could examine level spacings in a scaled version of the AISW. In the scaled AISW the ratio

$$\eta=V_0/E \tag{38}$$

is held fixed. For values of η slightly less than one we would expect to see nonuniform spacings, and it may be possible to carry out a meaningful statistical analysis of the sequence of spacings. Studies of the scaled AISW have revealed signatures of non-Newtonian orbits in the Fourier transform of the density of states [13], and recently an exact semiclassical theory for the eigenvalues of the scaled AISW has been developed [5]. Our hope is that more detailed study of both versions of the AISW will provide further insight into the influence of non-Newtonian periodic orbits on the properties of quantum systems.

[1] M. V. Berry and M. Tabor, Proc. R. Soc. London, Ser. A **356**, 375 (1977).

[2] O. Bohigas, M. J. Giannoni, and C. Schmit, Phys. Rev. Lett. **52**, 1 (1984).

[3] F. Haake, *Quantum Signatures of Chaos*, 2nd ed. (Springer, New York, 2001).

[4] M. C. Gutzwiller, *Chaos in Classical and Quantum Mechanics* (Springer, New York, 1990).

[5] A. S. Bhullar, R. Blümel, and P. M. Koch, Phys. Rev. E **73**, 016211 (2006).
[6] L. E. Reichl, *The Transition to Chaos: Conservative Classical Systems and Quantum Manifestations*, 2nd ed. (Springer, New York, 2004).
[7] H.-J. Stöckmann, *Quantum Chaos: An Introduction* (Cambridge University Press, New York, 1999).
[8] L. Couchman, E. Ott, and T. M. Antonsen, Phys. Rev. A **46**, 6193 (1992).
[9] R. Blümel, T. M. Antonsen, Jr., B. Georgeot, E. Ott, and R. E. Prange, Phys. Rev. Lett. **76**, 2476 (1996).
[10] R. Blümel, T. M. Antonsen, Jr., B. Georgeot, E. Ott, and R. E. Prange, Phys. Rev. E **53**, 3284 (1996).
[11] L. Sirko, P. M. Koch, and R. Blümel, Phys. Rev. Lett. **78**, 2940 (1997).
[12] A. Kohler, G. H. M. Killesreiter, and R. Blümel, Phys. Rev. E **56**, 2691 (1997).
[13] S. Bauch, A. Bledowski, L. Sirko, P. M. Koch, and R. Blümel, Phys. Rev. E **57**, 304 (1998).
[14] R. Schäfer, U. Kuhl, M. Barth, and H.-J. Stöckmann, Found. Phys. **31**, 475 (2001).
[15] R. N. Oerter, E. Ott, J. T. M. Antonsen, and P. So, Phys. Lett. A **216**, 59 (1996).
[16] M. A. Doncheski and R. W. Robinett, Eur. J. Phys. **21**, 217 (2000).
[17] L. P. Gilbert, M. Belloni, M. A. Doncheski, and R. W. Robinett, Eur. J. Phys. **26**, 815 (2005).
[18] Y. Dabaghian and R. Jensen, Eur. J. Phys. **26**, 423 (2005).
[19] W. H. Press, S. A. Teukolsky, W. T. Vetterling, and B. P. Flannery, *Numerical Recipes in FORTRAN 77*, 2nd ed. (Cambridge UP, Cambridge, 1992).
[20] M. V. Berry and M. Wilkinson, Proc. R. Soc. London, Ser. A **392**, 15 (1984).
[21] R. Blümel, Eur. J. Phys. **27**, L1 (2006).
[22] R. Bluhm, V. A. Kostelecký, and J. A. Porter, Am. J. Phys. **64**, 944 (1996).